JOURNAL OF MASS SPECTROMETRY, VOL. 33, 436–443 (1998)

Investigation of the *Trans* Effect in the Fragmentation of Dinuclear Platinum Complexes by Electrospray Ionization Surface-induced Dissociation Tandem Mass Spectrometry

Thomas G. Schaaff,† Yun Qu, Nicholas Farrell,* and Vicki H. Wysocki*‡
Department of Chemistry, Virginia Commonwealth University, 1001 West Main Street, Richmond, Virginia 23284, USA

Cis **and** ***trans*** **isomers of two dinuclear platinum complexes, [*cis*-{$Pt(NH_3)_2Cl$}$_2$μ-($NH_2(CH_2)_nNH_2$)]$(NO_3)_2$ (1,1/c,c) and [*trans*-{$Pt(NH_3)_2Cl$}$_2$μ-($NH_2(CH_2)_nNH_2$)]$(NO_3)_2$ (1,1/t,t), where the diamine was 1,4-butanediamine ($n = 4$) or 1,6-hexanediamine ($n = 6$), were studied using electrospray ionization surface-induced dissociation (ESI/SID) tandem mass spectrometry (MS/MS). The same fragment ions were observed for both the *cis* and *trans* isomers of each complex ($n = 4$ or 6), but the relative intensities were dependent on the isomer studied. The ESI/SID data and energy-resolved mass spectra show that the position of the chloride plays a significant role in the fragmentation of these ions. Two major fragmentation pathways were detected for the complexes. The cleavage of the Pt—N bond *trans* to chloride was the most favorable pathway for both isomers of the complexes following the ion–surface collision. The differences in the ESI/SID spectra between the *cis* and *trans* isomers can be explained by the *trans* effect, namely that the Pt—N bond *trans* to chloride is the most labile bond.** © **John Wiley & Sons, Ltd.**

J. Mass Spectrom. **33**, 436–443 (1998)

KEYWORDS: electrospray ionization; surface-induced dissociation; tandem mass spectrometry; dinuclear platinum complexes; *trans* effect

INTRODUCTION

Dinuclear platinum complexes of formula [{$Pt(NH_3)_2Cl$}$_2$μ-$NH_2(CH_2)_nNH_2$]$^{2+}$ are novel antitumor agents of clinical interest.[1,2] The presence of only one chloride on each platinum center means that the DNA binding of these species is bifunctional. We have previously reported on the conformational changes[3] and the interstrand[4] and intrastrand[5] cross-linking properties of [{*trans*-$Pt(NH_3)_2Cl$}$_2$μ-$NH_2(CH_2)_nNH_2$]$^{2+}$. The position of the chloride, either *cis* or *trans* to the diamine bridge, produces geometrical isomers and more recently the preparation, biological activity and DNA binding properties of the *cis* isomer, [{*cis*-$Pt(NH_3)_2Cl$}$_2$μ-$NH_2(CH_2)_nNH_2$]$^{2+}$, have been studied.[6,7] In contrast to the pair of mononuclear *cis*-/*trans*-$[Pt(NH_3)_2Cl_2]$ isomers, both *cis* and *trans* isomers in this dinuclear series display antitumor activity, but with different abilities to overcome cellular resistance to the 'parent' *cis*-$[Pt(NH_3)_2Cl_2]$.[6,8]

This paper describes a mass spectral (MS) investigation of *cis*- and *trans*-[{$Pt(NH_3)_2Cl$}$_2$μ-$NH_2(CH_2)_nNH_2$]$^{2+}$, where $n = 4$ and 6 (see Scheme 1). For many years, the mass spectral studies of transition metal complexes were limited to a select few types of complexes, e.g. metal carbonyls[9,10] and acetylacetonates.[11] This

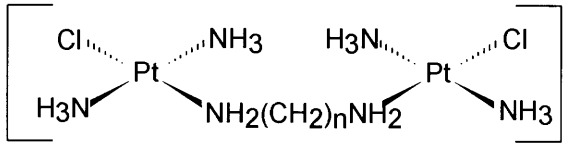

I 1,1/t,t n = 6
III 1,1/t,t n = 4

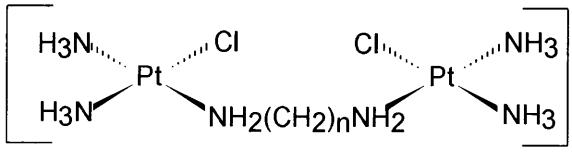

II 1,1/c,c n = 6
IV 1,1/c,c n = 4

Scheme 1. Structures of platinum complexes **I**, **II**, **III** and **IV**.

* *Correspondence to*: V. H. Wysocki, Department of Chemistry, University of Arizona, Tucson, Arizona 85721-0421, USA.
E-mail: vwysocki@u.arizona.edu
Contract grant sponsor: American Cancer Society. *Contract grant number*: DHP 2-E.
Contract grant sponsor: National Science Foundation. *Contract grant number*: CHE 9224719.
Contract grant sponsor: National Institutes of Health. *Contract grant number*: US DHHS, GM51387.
† *Present address*: School of Chemistry and Biochemistry, Georgia Institute of Technology, Atlanta, Georgia 30332-0430, USA.
‡ *Present address*: Department of Chemistry, University of Arizona, Tucson, Arizona 85721-0421, USA.

CCC 1076–5174/98/050436–08 $17.50

Received 24 April 1997
Accepted 9 January 1998

limitation resulted from both the low thermal stability of transition metal complexes and the lack of ionization methods that produce gaseous ions with sufficiently low internal energy to prevent fragmentation in the ionization source. Other techniques that have been employed more recently to study platinum complexes include fast atom bombardment (FAB),[12] matrix-assisted laser desorption/ionization (MALDI)[13] and field desorption.[14] Electrospray ionization[15] (ESI) was first developed for the study of large biopolymers, but has since been used for a variety of molecules. Recently, significant advances have been made in the field of ESI/MS of transition metal complexes. Colton and co-workers have excellent mass spectral data for platinum dithiolate complexes[16] and other transition metal complexes.[17] MALDI/MS has also been used to study the effects of metal–ligand bonds in oligonucleotides.[18]

In this paper, we show that electrospray ionization and surface-induced dissociation[19,20] (ESI/SID) tandem mass spectrometry (MS/MS) provides isomer distinction for the dinuclear platinum complexes investigated. Because the precursor ions of the isomers occur at the same m/z ratio, simple mass spectra of these compounds do not provide isomer distinction. SID studies involve collisions of mass-selected ions with a surface and the subsequent measurement of the relative abundances of fragment ions formed following the surface collision. SID has been performed on a variety of types of molecules including transition metal complexes. Metal carbonyls, such as $W(CO)_6^{+\cdot}$, have been used as 'thermometer' ions to determine the amount of internal energy deposited during ion–surface collisions.[9,10] These studies show that SID deposits large amounts of internal energy in a relatively narrow energy distribution.[21] It has been shown that the internal energy distribution provided by ion–surface collisions (SID) is narrower than the energy distribution associated with collisions of ions with gaseous targets such as He, Ar and Xe (CID).[22] The narrow energy distribution makes SID an attractive method for studying ion dissociation as a function of the internal energy deposition and allows for isomer distinction by the study of the energy dependence of fragmentation pathways.

One major motivation for this work is the desire to correlate gas-phase properties with those found in solution-phase chemistry. In the absence of solvent, it is possible to study the intrinsic chemical properties of the molecules. The *trans* effect has long been used to predict the reaction pathways of square-planar platinum complexes. In solution-phase chemical reactions, a Pt—N bond *trans* to a chloride is more labile than the corresponding bond *trans* to a nitrogen donor. As the data below show, application of the *trans* effect allows the prediction of the fragmentation pathways of various square-planar transition metal species in the gas phase.

EXPERIMENTAL

Synthesis of complexes

The synthesis of the dinuclear platinum complexes studied has been reported previously,[23,24] and the compounds were characterized by NMR, IR and elemental analysis.

The electrospray mass spectra show peaks at m/z 322 for the $n = 6$ diamine complexes (**I**, **II**) and m/z 308 for the $n = 4$ complexes (**III**, **IV**), corresponding to the doubly charged cation of each complex. Peaks corresponding to solvent adducts and impurities were visible in the mass spectra, but had low intensities relative to those of the ions of interest (less than 10% relative ion abundance).

Instrumental

The tandem mass spectrometer used for the ion–surface collisions was specifically designed to perform SID experiments.[21] The instrument consists of two Extrel 4000 u quadrupoles positioned at 90°. The ion beam intersects a surface at 45° with respect to the surface normal. The surfaces used for these experiments were perfluorinated alkanethiolate (2-perfluorooctylethanethiolate) self-assembled monolayer (SAM) films on vapor-deposited gold.[25] The electrospray source is a modified version of the Chait design[26] and the Knapp and Schey design.[27] The ESI/SID instrument used for these experiments has previously been used for studies involving large biological molecules[28,29] and *cis*-DDP bound to guanosine.[30] The potential difference between the capillary and skimmer was held constant at 40 V, unless gas-phase CID was desired. The pressure in this region was ~1 Torr (1 Torr = 133.3 Pa), as measured with an ion gauge located at the neck of the electrospray tee. The complexes were dissolved in 100% reagent-grade methanol at a concentration of ~10 pmol ml^{-1}. The sample was delivered with a syringe pump at a flow rate of 2 ml min^{-1}. The SID spectra were obtained for one structural isomer and then without changing the instrumental parameters, the other isomer was injected and an SID spectrum was obtained, providing identical instrument conditions for each isomer at each collision energy. To avoid sample carryover, the syringe was cleaned between loadings of the different isomers and, in several instances, a methanol blank was electrosprayed between infusions of the two isomers.

The potential applied to the skimmer was held at the same potential as the surface in order to obtain a simple single-stage mass spectrum.[21] The gas-phase positive ions produced by electrospray are transmitted to the first quadrupole. In order to obtain a simple mass spectrum, the ions are focused in a path to avoid collision with the surface and analyzed by the second quadrupole. To obtain *tandem* mass spectra, the first quadrupole is set to allow only the ions of interest to pass through (m/z 322 for $n = 6$ and m/z 308 for $n = 4$). With a zero potential difference between the skimmer and surface, the selected precursor ions pass by the surface into the second quadrupole and are detected. To induce dissociation, the potential on the surface is lowered and the selected ions collide with the surface. Upon collision, some of the kinetic energy of the projectile ion is transferred to internal energy, which initiates fragmentation. The fragment ions are then focused into the second

quadrupole and mass analyzed to obtain a surface-induced dissociation (SID) spectrum.

Because the dinuclear complexes of interest are doubly charged, the peaks in the mass spectrum were separated by 0.5 u. The entire envelope of isotopes of the precursor ion was selected and allowed to collide with the surface; however, all of the fragment ions detected were singly charged. In order to generate spectra as a function of collision energy (energy-resolved mass spectra; ERMS), the selected projectile ions were collided with the surface at different laboratory collision energies (40–80 eV). For doubly charged precursor ions, the actual laboratory collision energy is twice the potential difference between the skimmer and the surface, i.e. a 20 V potential difference created a 40 eV surface collision. The relative abundances of two major fragment ion groups (m/z 310 and 264 for $n = 6$ and m/z 282 and 264 for $n = 4$) are plotted against each collision energy.

To examine further the structure of the fragment ions and to probe the two-step fragmentation pathways, an additional means of fragmenting the ions was employed: the potential difference between the capillary and skimmer in the electrospray source was raised.[31] By raising the capillary voltage and holding the skimmer voltage constant, the ions were accelerated through the high-pressure region (~1 Torr) surrounding the capillary and skimmer. The accelerations and subsequent collisions with surrounding gaseous species caused fragmentation in the skimmer region. To assign the elemental composition of the fragment ions, the resolution of the second quadrupole mass analyzer was increased to 1 mass unit, to allow for the measurement of isotopic abundances of the elements present in the structures. Various fragment ions were then selected with the first quadrupole and collided with the surface, as explained above. Hence, two separate activation steps (ESI/CID/SID) allowed for the determination of the intermediate steps in the fragmentation processes.

RESULTS AND DISCUSSION

The gas-phase fragmentation behavior of *cis* and *trans* isomers of the platinum dinuclear complexes is presented here. The structures investigated (Scheme 1) will be referred to as **I** (1,1/t,t $n = 6$), **II** (1,1/c,c $n = 6$), **III** (1,1/t, t $n = 4$) and **IV** (1,1/c,c $n = 4$) for the remainder of this paper. Below, typical 50 eV electrospray ionization surface-induced dissociation (ESI/SID) spectra and capillary/skimmer CID mass spectra will be shown and the peaks identified, with the masses given referring to the ion containing the most abundant isotopes of each element present, i.e. ^{1}H, ^{12}C, ^{14}N, ^{35}Cl and ^{195}Pt. The elemental composition of the ions corresponding to the peaks in the ESI/SID spectra were assigned by comparing the observed isotope ratios with calculated ratios. Proposed fragmentation pathways of the complexes are described, and it is shown that all four complexes fragment by the same two major pathways. Different abundances for the fragment ions produced by the two pathways were observed for the *cis* and *trans* isomers. Finally, the energy-resolved mass spectra are presented to illustrate the differences in the fragmentation of the *cis* and *trans* isomers in a more explicit manner.

ESI/SID spectra

The ESI/SID spectra obtained for hexanediamine complexes, **I** and **II** [Fig. 1(a) and (b), respectively] show fragment ions corresponding to three different fragment

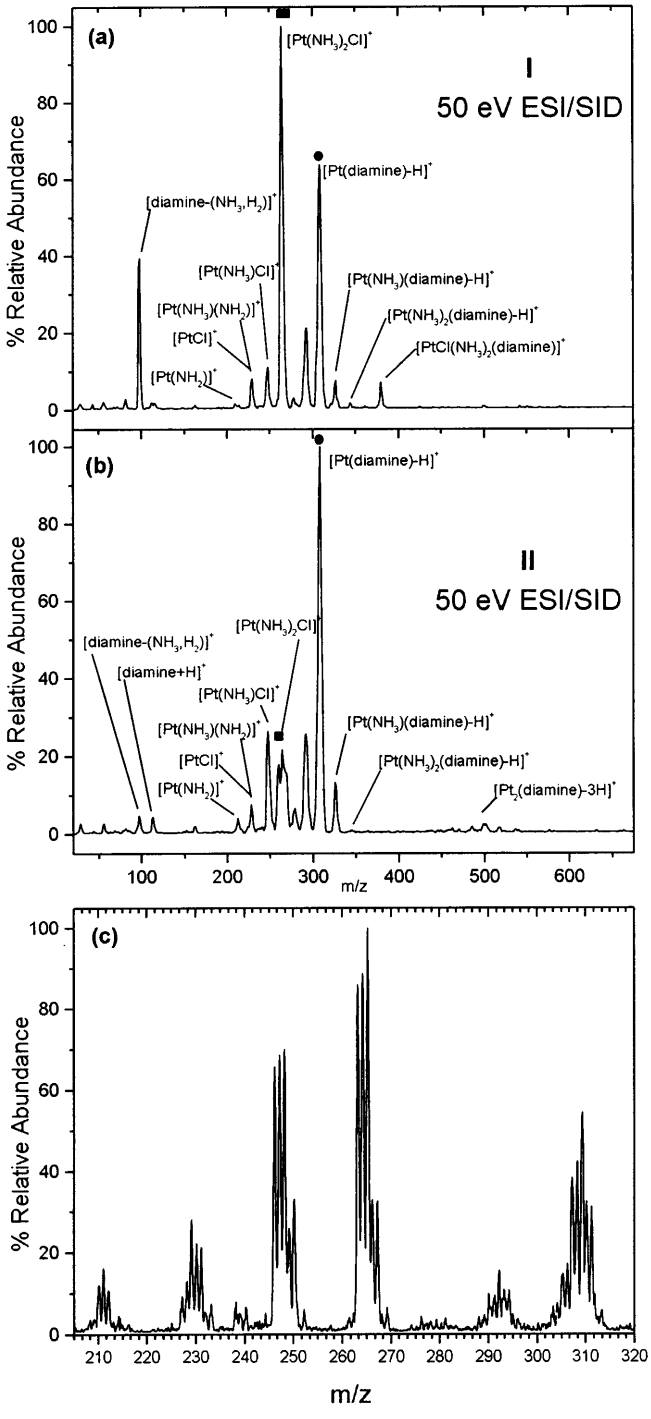

Figure 1. 50 eV ESI/SID collision spectra for the $n = 6$ complexes. Note the difference in the relative intensities of the fragment ions corresponding to the two pathways proposed in Scheme 2 (m/z 264 and 310) between complex **I** (a) and complex **II** (b), where the symbols denote the ions that will be used in ERMS. The capillary/skimmer CID spectrum of **I** (c) was used to determine the elemental formulae from the fragment ion isotope ratios.

ion groups. The selected doubly charged ion, $[\{Pt(NH_3)_2Cl\}_2\mu\text{-}NH_2(CH_2)_nNH_2]^{2+}$, was not visible in the collision spectra for either of the $n = 6$ complexes at any of the collision energies examined. The lower m/z ranges of the spectra (m/z 50–120) contain peaks corresponding to the fragments of the 1,6-hexanediamine ligand.[30] The remaining fragment ion groups are derived from two primary platinum containing fragment ions as shown in Scheme 2. The fragmentation pathway was determined for the complexes by a combination of capillary/skimmer CID experiments with SID experiments. All four complexes fragmented by the same pathways, generating fragment ions with equivalent structures differing only in the length of the diamine linkers.

The peak found at m/z 380, corresponding to the cleavage of one Pt—diamine bond and loss of the $[Pt(NH_3)_2Cl]^+$, was more intense for *trans* complex **I** than for *cis* complex **II**. By fragmenting the precursor ion in the capillary/skimmer region of the ESI source, it was possible to select this fragment ion (m/z 380) from the mass spectrum and determine that the fragments of this ion contribute to two different fragmentation pathways. When the second Pt—N(diamine) bond is dissociated, either the $[Pt(NH_3)_2Cl]^+$ or protonated diamine is formed. Alternatively, if the Pt—N(diamine) ligand is the only remaining ligand, the resultant ion is singly charged, suggesting a loss of H^+ as neutral HCl. This would allow for the possible chelation of the diamine through the other amino group. When the diamine is the only remaining ligand, the resultant ion exists as a singly charged ion, suggesting a loss of H^+. The group of ions found between m/z 300 and 350 are formed by the sequential losses of the two NH_3 groups after the loss of HCl. The ions from this process are $[Pt(NH_3)_2(NH(CH_2)_6NH_2)]^+$ (m/z 344), $[Pt(NH_3)(NH(CH_2)_6NH_2)]^+$ (m/z 327), and $[Pt(NH(CH_2)_6NH_2)]^+$ (m/z 310). These ions are further stabilized by rearrangement and loss of neutral H_2 groups, which can delocalize the charge; this is a common fragmentation process for aliphatic hydrocarbons.[32] The fragment at m/z 293 can be assigned as

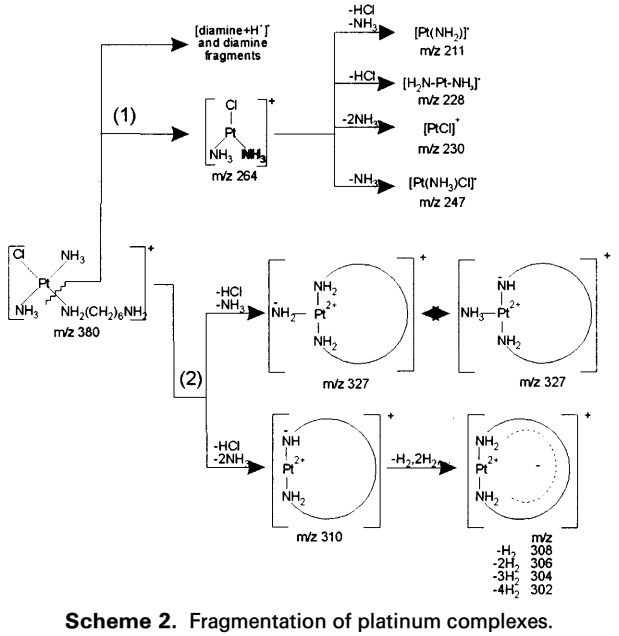

Scheme 2. Fragmentation of platinum complexes.

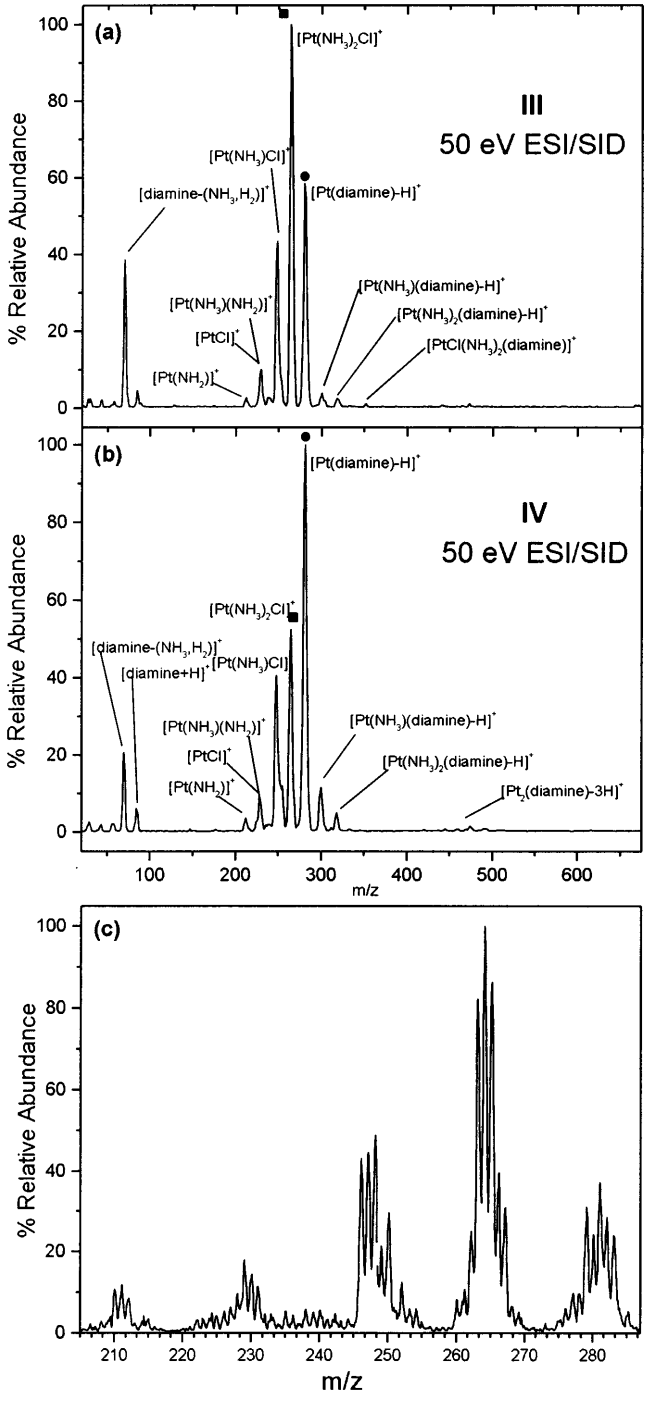

Figure 2. 50 eV ESI/SID collision spectra for the $n = 4$ complexes. As with the $n = 6$ complexes, pronounced differences in the relative abundances of fragment ions corresponding to the two pathways in Scheme 2 (m/z 264 and 281) are observed for complexes **III** (a) and **IV** (b). Again, the capillary/skimmer CID spectrum of **III** (c) was used to determine the elemental formulae.

$[Pt(NH(CH_2)_4CH{=}CH_2)]^+$, resulting from the fragmentation of the diamine by NH_3 loss, with retention of one Pt—N bond. The $[Pt(NH_3)_2Cl]^+$ fragment ion, when selected from the ion source and subjected to surface collisions, dissociates further to yield $[Pt(NH_3)Cl]^+$ (m/z 247), $[PtCl]^+$ (m/z 230), $[Pt(NH_3)(NH_2)]^+$ (m/z 228) and $[PtNH_2]^+$ (m/z 211). Again, the loss of HCl during the fragmentation process is a plausible explanation for the presence of the fragment ions at m/z 228 and 211.

Table 1. Isotope contributions for the $[Pt(NH_3)_2Cl]^+$ fragment ion found at *m/z* 261–269[a]

	261	263	264	265	266	267	269
Calculated	0.006	0.249	0.256	0.272	0.084	0.116	0.018
Measured	0.009	0.262	0.257	0.267	0.074	0.112	0.019

[a] Relative abundances of less than 0.0005 were not used for determination (i.e. *m/z* 262, 268).

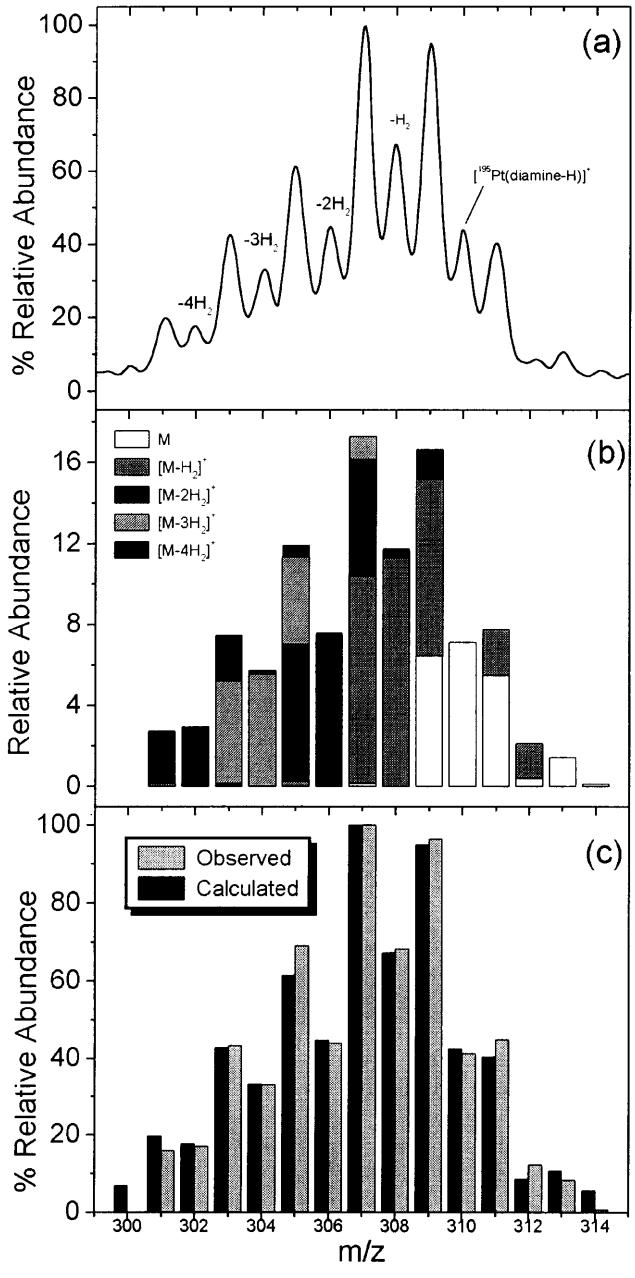

Figure 3. Isotope pattern of fragments found at *m/z* 300–313, corresponding to the fragment ions formed in pathway (2) (Scheme 2) for the $n = 6$ complexes (**I** and **II**). (a) Observed isotope pattern for the fragment ions. Note the increased relative abundance at 2 mass units apart due to the overlap of a fragment ion containing ^{194}Pt and a fragment ion containing ^{196}Pt after loss of H_2. (b) Graphical representation of the method used to sum the different peaks corresponding to isotopes of different fragment ions produced by the loss of H_2. (c) Comparison of calculated abundances and observed abundances, after the outlined procedure is followed.

The fragment ions observed for the *cis*- and *trans*-butanediamine complexes, **III** and **IV** [Fig. 2(a) and (b)] correspond to those found in the $n = 6$ counterparts (**I** and **II**, respectively). A peak corresponding to the protonated diamine ligand was observed and the fragments from the diamine are also observed, as with the $n = 6$ complex. [Separate experiments were performed using ESI and SID of 1,6-hexanediamine and 1,4-butanediamine. The protonated ions of 1,6-hexanediamine (*m/z* 117) and 1,4-butanediamine (*m/z* 89) were dissociated. The fragment ions of 1,6-hexanediamine were $NH_2(CH_2)_6^+$ (*m/z* 100), $NH_2CH_2^+$ (*m/z* 30) and other low-abundance ions corresponding to dissociation of C—C bonds. For 1,4-butanediamine the fragments were $NH_2(CH_2)_4^+$ (*m/z* 72) and $NH_2CH_2^+$ and also with fragmentation of the C—C bonds.] At *m/z* 264, the peak representing the structure $[Pt(NH_3)_2Cl]^+$ was detected. The peaks corresponding to the fragments from this structure are seen at *m/z* 247, 230, 228, and 211 (formulae are listed above). The proposed diamine ring fragment ion, $[Pt(diamine\text{-}H)]^+$ appears at *m/z* 282. At 17 mass units above that, *m/z* 299, the fragment ion is $[PtNH_3(diamine\text{-}H)]^+$. The contribution to the intensity of the peak at *m/z* 264–267 is from two fragment ions. Based on comparison with the $n = 6$ complexes and the isotope abundances of the ions [Fig. 1(c)], one fragment ion is $[Pt(NH_3)_2Cl]^+$ (*m/z* 264). The other is assigned as $[Pt(NH_2(CH_2)_2CH{=}CH_2)]^+$ (*m/z* 266), based on the corresponding fragment ion for the $n = 6$ complexes being found at *m/z* 294.

There are two major differences between the SID spectra of the *cis* and *trans* isomers of either the $n = 4$ or $n = 6$ complex: (i) the intensity of the $[Pt(NH_3)_2Cl]^+$ fragment for the *trans* complexes **I** and **III** was greater throughout all collision energies studied and (ii) the relative abundances of the fragment ions $[Pt(NH_3)_2Cl]^+$ (*m/z* 264) and $[Pt(diamine\text{-}H)]^+$ [*m/z* 310 (**I**) and *m/z* 282 (**III**)] differ considerably depending on which isomer is being studied.

Fragment ion formula assignment

Because of the large number of platinum isotopes and the possible presence of chlorine with its two isotopes, special attention is required in the determination of fragment ion composition. To identify the fragment ions, capillary/skimmer CID was employed and the resolution of the second mass analyzer was increased to unit mass resolution (the resultant spectra are shown in Figs 1(c) and 2(c) for $n = 6$ and 4, respectively). The platinum and chlorine isotopic abundances allowed for straightforward determination of elemental composition

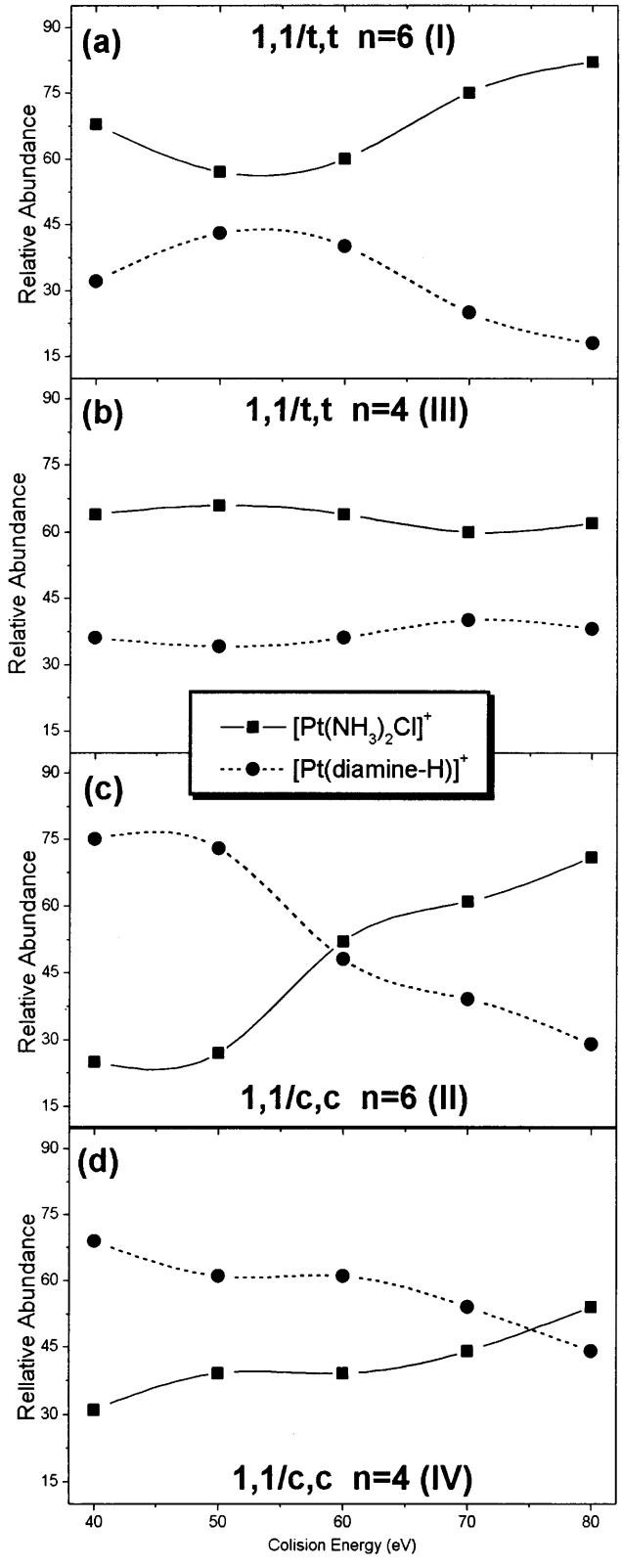

Figure 4. Energy-resolved mass spectra for all of the complexes. Note that the general shape for like isomers is the same. For the *trans* isomers of $n = 6$ (a) and $n = 4$ (b), $[Pt(NH_3)_2Cl]^+$ was the most abundant of the two ions over all energies studied. However, for the *cis* isomers of $n = 6$ (c) and $n = 4$ (d), at lower collision energies the $[Pt(diamine\text{-}H)]^+$ ion was more abundant, then at a certain critical energy the most abundant ion became the $[Pt(NH_3)_2Cl]^+$ ion. The fragment ion abundances used for the breakdown curve correspond to the two major fragmentation pathways proposed in Scheme 2.

Table 2. Isotope contributions for $[Pt(diamine\text{-}H^+)]^+$ and $[Pt(diamine\text{-}H^+)(-H_2, -2H_2, \ldots)]^+$ fragment ions appearing at *m/z* 301–314[a]

m/z	M	M − H_2	M − $2H_2$	M − $3H_2$	M − $4H_2$	Relative abundance (%)
301				0.120	2.620	2.67
302					2.950	2.87
303			0.161	5.036	2.272	7.28
304				5.560	0.165	5.58
305		0.243	6.802	4.282	0.591	11.61
306			7.510	0.031	0.045	7.39
307	0.153	10.22	5.784	1.114		16.83
308		11.29	0.420	0.085		11.49
309	6.449	8.696	1.500			16.22
310	7.120	0.631‡	0.113‡			6.94
311	5.484	2.261				7.55
312	0.398	1.730				2.07
313	1.426					1.39
314	0.109					0.11

[a] The relative abundances shown for each fragment were calculated as prescribed in the text. The isotope contributions for the fragments were summed for each *m/z* and the summed values were normalized to unity to produce the relative abundance.

of most fragment ion structures, such as the $[Pt(NH_3)_2Cl]^+$ fragment ion (Table 1). For more complicated situations, e.g. the fragment ions found at approximately *m/z* 310 (**I** and **II**) and *m/z* 282 (**III** and **IV**), simple inspection of isotope contributions was not possible and calculations were required

One way to explain the unusual broad grouping at *m/z* 301–314 for $n = 6$ and *m/z* 276–286 for $n = 4$ is that multiple H_2 losses occur in the $[Pt(diamine\text{-}H)]^+$ ion. Calculations were performed to allow comparison of calculated and observed ratios to explore this possibility. With the loss of H_2, overlapping of platinum isotope peaks occurs. As an example, we use the fragment ions of **I** found at *m/z* 301–314 in the ESI/SID spectra [Fig. 3(a)], where the normal platinum isotope pattern for ^{195}Pt, ^{196}Pt and ^{198}Pt isotopes was discernible for *m/z* 310, 311 and 313. Table 2 shows the calculated abundances of each isotope of each fragment, if consecutive losses of H_2 are assumed. The calculated abundances are shown graphically as summed bars in Fig. 3(b). The highest *m/z* fragment containing ^{195}Pt (*m/z* 310) was used as a reference and normalized to the other observed peaks (between *m/z* 301 and 314). Assuming that one fragment was $[^{195}Pt(diamine\text{-}H)]^+$, the peak found at *m/z* 309 would have a relative abundance due to the contribution from both the $[^{194}Pt(diamine\text{-}H)]^+$ ion and the $[^{196}Pt(diamine\text{-}H) - H_2]^+$ ion, i.e. after the loss of H_2. Therefore, the abundance of the $[^{194}Pt(diamine\text{-}H)]^+$ ion (based on the observed intensity of the $[^{195}Pt(diamine\text{-}H)]^+$ fragment) was subtracted from the observed abundance at *m/z* 309, giving the relative abundance of the $[^{196}Pt(diamine\text{-}H) - H_2]^+$ ion (after H_2 loss). The calculated intensity of the peak due to the $[^{196}Pt(diamine\text{-}H) - H_2]^+$ ion was used to normalize the abundances of the other platinum isotopes in the H_2 loss fragment ions. Then, using the calculated $[^{195}Pt(diamine\text{-}H) - H_2]^+$ abundance (based on $[^{196}Pt(diamine\text{-}H)$

$-H_2]^+$ abundance), the steps were repeated for the $-2H_2$, $-3H_2$ and $-4H_2$ fragment ions. The abundances at each m/z were summed and normalized. The calculated spectrum matched the observed spectrum with an average error of ~4% [Fig. 3(b)]. A similar calculation was performed for the $n = 4$ compounds and showed a comparable average error; of course, for $n = 4$ fewer total H_2 molecules can be lost [e.g. see Figs 1(c) and 2(c) to compare the envelopes]. When spectra were obtained as a function of collision energy, the envelopes shifted to lower m/z, consistent with the loss of a greater number of H_2 with an increase in energy.

Energy-resolved mass spectra

To summarize the main pathways described above, dissociation of one Pt—N(diamine) bond, resulting in two singly charged ions, occurs for all of the complexes studied. In the next step of the fragmentation pathway, either (**1**) the other Pt—N(diamine) bond is cleaved or (**2**) the Pt—N(diamine) bond is retained and the other ligand bonds are cleaved (Scheme 2). Note that in the spectra for the complexes, the relative intensities of the peaks corresponding to $[Pt(NH_3)_2Cl]^+$ and $[Pt(diamine\text{-}H)]^+$ are different for the *cis* and *trans* isomer of each complex. This is even more apparent when the relative abundances for the key product ions are plotted as a function of collision energy (ERMS, Fig. 4).

Just as other spectroscopic techniques use a range of absolute energies, isomer distinction by MS/MS uses a series of collision energies that can be used to show differences inherent in the structures being studied. For precursor ions with the same chain length n, the peaks in the ESI/SID spectra are at the same m/z ratio, but with different intensities. This can be immediately recognized, for example, in Figs 1 and 2, where the symbols over the ions of interest correspond to the symbols used in ERMS. Because the ions $[Pt(NH_3)_2Cl]^+$ and $[Pt(diamine\text{-}H)]^+$ are the major products produced by the fragmentation of the *cis* and *trans* complexes, the abundances of these two ions were used to generate the ERMS. Recall that, in the case of **III** and **IV**, the cluster of peaks found at m/z 264 was due to the overlap of two fragment ions, $[Pt(NH_3)_2Cl]^+$ and $[Pt(NH(CH_2)_2CH{=}CH_2)]^+$. Even though corrections for the overlap were not made, the general features of the ERMS plots for $n = 4$ (**III** and **IV**) are in good agreement with the corresponding plots for the $n = 6$ counterparts (**I** and **II**) (Fig. 4).

The ERMS plot for the hexanediamine complex, **I** [Fig. 4(a)] shows that at all collision energies the preferred dissociation pathway for the *trans* complex is the dissociation of both Pt—N(diamine) bonds, *trans* to chloride, in the proposed stepwise manner. Likewise, the same trend is observed for **III** [Fig. 4(b)]. In contrast, at lower collision energies the preferred dissociation pathway for both *cis* isomers, **II** [Fig. 4(c)] and **IV** [Fig. 4(d)], is the dissociation of one Pt—N(diamine) bond followed by the retention of the second Pt—N(diamine) bond. For both **II** and **IV**, a collision energy is reached at which the preferred pathway becomes the generation of the $[Pt(NH_3)_2Cl]^+$ ion.

CONCLUSIONS

The *trans* effect of ligands in a square-planar complex is generally used to describe chemical reactions in the solution phase where the most labile bond in these complexes would be the Pt—N bond *trans* to chloride. Our data suggest that the position of the chloride also plays an integral role in the gas-phase fragmentation of these complexes, independent of incoming solvent effects. It is observed that when the chloride is *trans* to the diamine linker (as in **I** and **III**) the preferred pathway is to cleave **both** of the *trans*-Pt—N(diamine) bonds, producing a dominant $[Pt(NH_3)_2Cl]^+$ fragment ion over all energies studied. The gas-phase *trans* effect is further supported by the fragmentation pathway for **II** and **IV**. In these complexes, the chloride is now *cis* to the diamine linker, resulting in a more labile Pt—NH_3 bond instead of the Pt—N(diamine) bond. In both **II** and **IV**, the preferred fragmentation pathway at lower collision energies is dissociation of one Pt—N(diamine) bond and retention of the other Pt—N(diamine) bond. Because the chloride is in the *cis* position, the abstraction of the proton from the diamine is a kinetically favored process and the proposed $[Pt(diamine\text{-}H)]^+$ structure can be formed. This structure fragments further by loss of H_2 and may form a bidentate ring structure with the platinum. Eventually, an energy is reached at which the preferred pathway is the dissociation of both Pt—N(diamine) bonds. At higher energies, the steric effects of the ligands of the complex may outweigh any stabilizing effects inherent from the *trans* effect of the chloride.

With the advances being made in ionization and activation techniques in mass spectrometry, fundamental studies of transition metal systems are becoming more viable. Our results show that the use of ESI in conjunction with SID is a very useful combination for this class of metal complex ions. Also, the ESI/SID data allowed a correlation to be made between solution-phase characteristics of transition metal complexes and the observable gas-phase characteristics. By studying the gas-phase fragmentation characteristics, the intrinsic properties of the ions can be probed. ESI provides projectile ions with sufficiently low internal energy to prevent fragmentation in the source and SID provides an internal energy deposition with a narrow energy distribution. With this combination, differences in the energy-dependent fragmentation pathways can be detected. This allowed the observation of differences in fragmentation pathways due to the *trans* effect of the chloride in the dinuclear complexes. Simple single-stage mass spectrometry would not allow for the determination of the structural isomers of transition metal complexes, but ESI/SID provided data that permitted the distinction of structural isomers from the differences in the fragmentation patterns of those isomers.

Acknowledgement

This work was supported by the American Cancer Society (DHP 2-E), National Science Foundation (CHE 9224719) and National Institutes of Health (US DHHS, GM51387). We thank Ronald J. Wysocki, Jr, for assistance with the manuscript.

REFERENCES

1. N. Farrell, *Comments Inorg. Chem.* **16**, 373 (1995).
2. N. Farrell, in *Advances in DNA Sequence Specific Agents*, edited by L. H. Hurley and J. B. Chaires, Vol. 2. JAI Press, Greenwich, CT, **2**, 187 (1996).
3. A. Johnson, Y. Qu, B. Van Houten and N. Farrell, *Nucleic Acids Res. 20*, 1697 (1992).
4. Y. Zo and B. Van Houten, Farrell, N. *Biochemistry* **33**, 5404 (1994).
5. M. J. Bloemink, J. Reedijk, N. Farrell, Y. Q and A. I. Stetsenko, *J. Chem. Soc., Chem. Commun.* 1002 (1992).
6. N. Farrell, T. G. Appleton, A. P. Soares-Fontes, Y. Qu, P. W and Y.Zou, *Biochemistry* **34**, 15890 (1996).
7. K. J. Mellish, Y. Qu, J. Scarsdale and N. Farrell *Nucleic Acids Res*. **25**, 1265 (1997).
8. C. Manzotti, G. Pezzoni, F. Giuliani, M. Valsecchi, N. Farrel and S. Tognella, *Proc. AACR* **35**, 2628 (1994).
9. V. H. Wysocki, H. I. Kenttäma and R. G. Cooks, *Int. J. Mass Spectrom. Ion Processes* **75**, 181 (1987).
10. S. A. Miller, D. E. Piederer, Jr, R. G. Cooks, W. R. Cho, H. W. Lee and H. Kang, *J. Phys. Chem.* **98**, 245 (1994).
11. J. Charalambous, R. G. Copperthwaite, S. W. Jeffs and D. E. Shaw, *Inorg. Chim. Acta* **14**, 53 (1975).
12. I. A. G. Roos, A. J. Thompson and J. Eagles, *Chem. Biol. Interact. 8*, 421 (1974).
13. J. P. Macquet, K. Jankowski and J. L. Butor, *Biochem. Biophys. Res. Commun.* **92**, 68 (1980).
14. J. Claereboudt, B Spiegeleer, E. A. De Bruijn, R. Gijbels and M. Claeys, *J. Pharm. Biomed. Anal.* **7**, 1599 (1989).
15. J. B. Fenn, M. Mann, C. K. Meng, S. F. Wong and C. M. Whitehouse, *Science* **246**, 64 (1989).
16. R. Colton, V. Tedesco and J. Traeger, *Inorg. Chem.* **31**, 3865 (1992).
17. A. Bond, R. Colton, Y. Mah and J. Traeger, *Inorg. Chem.* **33**, 2548 (1994).
18. C. E. Costello, K. M. Comess, A. S. Plaziak, D. P. Bancroft and S. J. Lippard, *Int. J. Mass Spectrom. Ion Processes* **122**, 255 (1992).
19. R. G. Cooks, T. Ast, T. Pradeep and V. Wysocki, *Acc. Chem. Res. 27*, 316 (1994).
20. R. G. Cooks, T. Ast and Md. A. Mabud, *Int. J. Mass Spectrom. Ion Processes* **100**, 209 (1990).
21. V. H. Wysocki, J. Ding, J. L. Jones, J. H. Callahan and F. L. King, *J. Am. Soc. Mass Spectrom.* **3**, 27 (1992).
22. K. Vékey, Á. Somogyi and V.H. Wysocki, *J. Mass Spectrom. 30*, 212 (1995).
23. H. Rauter, D. R. Domenico, E. Menta, A. Oliva, Y. Qu and N. Farrell, *Inorg. Chem*. **36**, 3919 (1997).
24. Y. Qu and N.J. Farrell, *J. Inorg. Biochem.* **40**, 255 (1990).
25. Á. Somogyi, T. E. Kane, M. Ding and V.H. Wysocki, *J. Am. Chem. Soc.* **115**, 5275 (1993).
26. S. K. Chowdhury, V. Katta and B. T. Chait, *Rapid Commun. Mass Spectrom.* **4**, 81 (1990).
27. D. I. Papac, K. L. Schey and D. R. Knapp, *Anal. Chem.* **63**, 1658 (1991).
28. J. L. Jones, A. R. Dongre, Á. Somogyi and V. H. Wysocki, *J. Am. Chem. Soc.* **116**, 8368 (1994).
29. A. L. McCormack, Á. Somogyi, A. R. Dongre and V. H. Wysocki, *Anal. Chem.* **65**, 2859 (1994).
30. T. G. Schaaff, Y. Qu, N. Farrell and V. H. Wysocki, in *Proceedings of the 42nd ASMS Conference on Mass Spectrometry and Allied Topics*, Chicago, IL, 29 May –3 June 1994.
31. J. B. Fenn, *J. Am. Soc. Mass Spectrom.* **4**, 524 (1993).
32. K. L. Busch, G. L. Glish and S. A. McLuckey, *Mass Spectrometry/Mass Spectrometry*: *Techniques and Applications of Tandem Mass Spectrometry*. VCH, New York (1988).